Nonlinearity-Robust IM/DD THz Communication System via Two-Stage Deep Learning Equalizer

Pouya Torkaman, Seyed Mostafa Latifi, Kai-Ming Feng, *Member, IEEE*, and Shang-Hua Yang, *Senior Member, IEEE*

***Abstract*— Linear and nonlinear impairments restrict the transmission performance of high-speed terahertz (THz) communication systems. To improve transmission performance, we propose a two-stage nonlinear equalizer (NLE). In the first stage, a memory-controlled long short-term memory (LSTM) neural network learns channel nonlinearity and compensates for it through nonlinear waveform regression. In the second stage, a low-complexity deep random forest (RF) network identifies nonlinear boundaries among individual QAM symbols and adjusts the standard hard decision thresholds of the QAM demodulator to align with the distribution of received symbols. This study experimentally validates the proposed two-stage NLE on a dual-channel THz-over-fiber transmission system using an intensity modulation and direct detection (IM/DD) scheme, achieving a successful 20 Gbps line rate up to a 4.5-meter wireless link at both 125/300 GHz frequency bands. The proposed scheme outperforms a Volterra nonlinear equalizer in all tested scenarios, surpassing a linear equalizer (LE) by reducing the bit error rate (BER) from 2.47×10^{-3} to 2.61×10^{-4} in the 300 GHz link and from 3.42×10^{-3} to 5.64×10^{-4} in the 125 GHz link.**

***Index Terms*— THz communication, OFDM, IM/DD, artificial intelligence, non-linear equalizer, LSTM.**

I. Introduction

THE rapid advancements in cloud computing, artificial intelligence, and the internet of things challenge the bandwidth and data rates supported by 5G technology, especially given its reliance on constrained millimeter-wave spectrum. To deal with the rising capacity needs of data-intensive applications, the terahertz (THz) band, with its rich spectrum resources, is explored for future 6G communications [1], [2]. Among the diverse technologies for THz communication, the photomixing method is particularly appealing due to its compatibility with existing fiber communication through THz-over-fiber technology and broad spectrum range tunability, facilitating the seamless integration of THz communication systems with current communication networks [3]. Over the past decade, there has been a notable increase in the experimental demonstration of photomixer-based THz communication systems with wireless data rates ranging from few Mbps to 100s of Gbps [4], [5], [6], [7]. In these systems, advanced modulation formats, including quadrature amplitude modulation (QAM) formats used in both single-carrier [4], [5] and multi-carrier orthogonal frequency division multiplexing (OFDM) formats [6], [7], are applied to improve spectral efficiency and, consequently, achieve higher data rates. Moreover, OFDM demonstrates robust resistance to THz channel impairments, facilitating the acquisition of channel state information and symbol detection compared to a single-carrier system; nevertheless, coherent detection is typically required for achieving high data rates. This involves sub-harmonic radio frequency mixing with a frequency multiplier, significantly increasing the system's complexity and hindering practical implementation. In contrast, a direct detection approach for THz communication, which involves a low-hardware-complexity, time-resolved THz receiver to capture the signal envelope of an intensity-modulated THz signal, offers a straightforward solution. Unfortunately, linear and nonlinear distortions originated from various system elements such as the Mach-Zehnder modulator (MZM), optical and electrical amplifiers, along with subcarrier-to-subcarrier-beating interference (SSBI) induced by square detection, present a significant constraint on intensity modulation direct detection (IM/DD) OFDM transmission which are theoretically quantified in [7], [8], and [9]. Therefore, advanced equalization methodologies play a pivotal role in enhancing system performance and meeting the demands of THz communication systems.

With the advancement of artificial intelligence, the neural network has been adopted as the advanced equalization scheme, leveraging their robust learning and nonlinear mapping capabilities [10], [11], [12], [13]. However, the computational complexity associated with multi-layer equalizers [10], [11], [12], and the necessity for a substantial amount of training symbols for equalization tasks on received symbols impose constraints on their application in high-speed THz communication [13].

In this letter, we propose a two-stage deep learning-assisted nonlinear equalizer designed to counteract nonlinear distortions effectively. In the first stage, the received sampled time-domain OFDM signal is fed into a memory-controlled long short-term memory (LSTM) unit for nonlinear wave regression. Given that THz wireless systems operate with highly directional beams under line-of-sight (LOS) conditions, the impact of multi-path fading is negligible, enabling equalization in the time domain with reasonable complexity. Additionally, equalizing the received signal in the time domain before subsequent processing routines avoids complex value training and preserves the linear and nonlinear connections between sample points, facilitating the equalizer in discerning patterns of nonlinearity without requiring multi-layer networks. In the second stage, a random forest (RF) equalizer undergoes training to discern the optimal nonlinear boundaries for QAM symbol classification. It categorizes each received symbol into one of the M groups based on

Manuscript received 1 May 2024; accepted 19 June 2024. Date of publication 24 June 2024; date of current version 14 August 2024. The associate editor coordinating the review of this letter and approving it for publication was O. Simpson. *(Corresponding author: Shang-Hua Yang.)*

Pouya Torkaman, Seyed Mostafa Latifi, and Shang-Hua Yang are with the Institute of Electronics Engineering, National Tsing Hua University, Hsinchu 300, Taiwan (e-mail: Torkaman.pouya@gmail.com; seyed@liverpool.ac.uk; shanghua@ee.nthu.edu.tw).

Kai-Ming Feng is with the Institute of Communication Engineering, National Tsing Hua University, Hsinchu 300, Taiwan (e-mail: kmfeng@ee.nthu.edu.tw).

Digital Object Identifier 10.1109/LCOMM.2024.3418457

© 2024 The Authors. This work is licensed under a Creative Commons Attribution-NonCommercial-NoDerivatives 4.0 License.
For more information, see https://creativecommons.org/licenses/by-nc-nd/4.0/

the modulation format, thereby equalizing the channel and accomplishing the equalization task with ultra-low complexity. Furthermore, to evaluate the performance of the uni-traveling-carrier photodiode (UTC-PD) and pin-photodiode (PIN-PD) as the two most established optoelectronic THz emitters, we configured a dual-channel IM/DD OFDM THz communication system. This system delivered OFDM signals at the optimal operating frequency of each THz emitter. Using this setup, we experimentally validated the proposed two-stage nonlinear equalizer with a 16-QAM 5 Gbaud OFDM signal, considering the limited THz detector bandwidth.

II. Dual-Channel IM/DD THz Communication System

Fig.1 illustrates the setup of the dual-channel THz communication system. It incorporates three tunable distributed feedback (DFB) laser diodes operating in the C-band. LD-1 generates the optical carrier signal at 1550 nm, while LD-2 and LD-3, serving as local oscillators, generate optical signals at 1551 nm and 1552.4 nm, respectively. The optical signal from LD-1 passes through a polarization controller before being routed to a single-drive Mach-Zehnder modulator (MZM) for performance optimization. Pre-generated 16-QAM 5 Gbaud OFDM signals, used to modulate the optical carrier in the MZM, are created offline using MATLAB code and then converted to analog form by an arbitrary waveform generator (AWG). To counteract MZM and optical link losses while boosting overall optical power, the signal undergoes amplification via an erbium-doped fiber amplifier (EDFA). Additionally, an accompanying band-pass filter is employed to eliminate any out-of-band amplified spontaneous emissions.

The amplified modulated signal is split into two equal-power signals, each then combined with a respective local oscillator. In the 125 GHz link, the optical signal is directed to a PIN-PD for x-polarized THz signal generation. In the 300 GHz link, the signal is directed to a UTC-PD for y-polarized THz signal generation. With orthogonal polarizations in the two links, radiated waves from one link do not interfere with the other.

In both links, polarization controllers precede heterodyning for enhanced polarization-dependent conversion of THz emitters. In our experiment, optical power is set to be 12 dBm in both links for consistent device performance during long testing trials. Each link in the free-space THz datalink integrates a pair of THz lenses for collimating the THz beam and minimizing propagation losses. At the receiver end, two Fermi-level managed barrier (FMB) diodes, each positioned to detect a specific polarization, serve as envelope detectors. The received THz signals are then captured by a high-speed real-time digital oscilloscope. Following this, a digital signal processing (DSP) algorithm is applied offline, encompassing down-conversion, channel estimation, equalization, phase noise compensation, and digital demodulation.

III. Two-Stage Nonlinear Equalizer

Here, we propose the two-stage NLE to estimate and compensate for nonlinear impairments in THz communication systems. As presented in Fig.1, the first stage of the proposed NLE features a memory layer and representative delay units (z^{-1}) that store present and preceding OFDM samples. Prior to equalization, The OFDM samples are resampled and time-synchronized to ensure the window begins with the correct samples. The training sequence is then extracted from the overall signal and utilized to train the model. The first post-equalization stage utilizes a prolonged sequence model, aiming to correlate the current output with the output states of previous moments. For this purpose, we adopt an LSTM network with H hidden units, which retains persistent memory across multiple sessions. It prioritizes the latest data sequence and maintains weights from the original model during training. This lasting memory significantly enhances the LSTM's ability to compensate for nonlinear impairments through waveform regression in the time domain. It is worth noting that the first equalization stage is insensitive to the order of QAM and can be directly applied to higher-order modulation formats.

Each LSTM unit encompasses a forget gate f_n determining which information to discard, an input gate i_n responsible for storing content in the cell, and an output gate o_n regulating the information to be transmitted. The forward pass LSTM cell equations for a time-step n can be concisely expressed as follows [14]:

$$\begin{aligned} f_n &= \sigma(w_f x_n + R_f h_{n-1} + b_f) \\ i_n &= \sigma(w_i x_n + R_i h_{n-1} + b_i) \\ o_n &= \sigma(w_o x_n + R_o h_{n-1} + b_o) \\ C_n &= f_n \odot C_{n-1} + i_n \odot \tanh(w_c x_n + R_c h_{n-1} + b_c) \\ h_n &= o_n \odot \tanh(C_n) \end{aligned} \tag{1}$$

where $w_{f,i,o,c}$, $R_{f,i,o,c}$, and $b_{f,i,o,c}$ vectors represent input weights, recurrent weights, and biases, respectively, which are trainable variables. σ denotes the logistic sigmoid activation function and $\odot$ is the element-wise product operand.

The stored temporal data sequence from the received OFDM signal has the following form: $x_{n,L} = [x_{n-k}, \ldots, x_{n-1}, x_n]$, where L represents the overall length of the sequence which is equal to $L = k + 1$. Thus, at discrete time n, we feed k preceding samples into the LSTM network to capture system nonlinearities and establish temporal relationships among adjacent samples. Following this, a single feedforward layer systematically maps the weighted output of each LSTM cell, providing an accurate estimate of the intact OFDM signal.

After waveform correction, the signal undergoes down-conversion and low-pass filtering to capture the baseband signal. The fast Fourier transform (FFT) block transforms the time-domain OFDM signal into the frequency domain for the second equalization stage to perform equalization at the sub-carrier level. In contrast to the first equalization stage, where LSTM networks aim to compensate for channel nonlinearity by minimizing the mean square error (MSE) of sequential sample points in the OFDM signal, the second stage operates on the distributions of the entire training set rather than individual data sequences. Its goal is to minimize the entropy of the training set and align hard decision boundaries with the distributions of received QAM symbols, leveraging prior knowledge of the location of each QAM symbol. This is accomplished by combining a linear equalizer (LE) with an ultra-low complexity learning-based random forest (RF). The RF determines decision boundaries and classifies symbols into 16 groups based on modulation format.

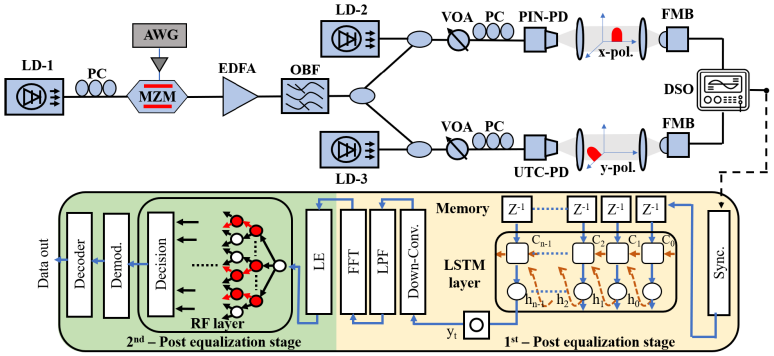

Fig. 1. Dual channel THz communication system with proposed two-stage NLE. PC: Polarization controller. MZM: Mach-Zehnder modulator. OBF: Optical band-pass filter. EDFA: Erbium-doped fiber amplifier. FMB: Fermi-level managed barrier diode. DSO: Digital storage oscilloscope.

The RF classifier employs bootstrap aggregation to construct a model through an ensemble of decision trees. This process involves growing classification trees on a random subset of features, with node categorization determined by considering the entropy-based splitting rule [15]. In our 16-QAM OFDM THz communication system, the input features, denoted as $N = \{N_1, N_2\}$, represent the in-phase and out-of-phase components of each QAM symbol, while the candidate set for category information is denoted as $C = \{C_1, C_2, C_3, \ldots, C_{16}\}$. The classification entropy can be calculated as follows:

$$H(D) = -\sum_{m=1}^{M} P(y = C_m) \log_2 P(y = C_m) \tag{2}$$

where, $P(y = C_m)$ represents the proportion of training data associated with category C_m relative to the entire training dataset. In the training process, the goal is to identify the optimal decision boundary. This is achieved by calculating entropy before and after splitting the nodes, resulting in the computation of Information Gain (IG) from each individual split using assigned thresholds for each feature. IG can be formulated as:

$$IG(D, N_i^v) = H(D) - H(D|N_i^v) \tag{3}$$

where N_i^v represents the different values of selected feature. The condition with the highest IG is selected as the root node of the decision tree. This splitting process continues until the leaf nodes are accurately categorized and decision boundaries are finalized.

In RF, the number of decision trees (N) and their depth (D) are critical hyperparameters. Choosing too few trees leads to coarse decision boundaries and reduced accuracy, while an excessively large number increases complexity and training time. Striking the right balance is essential for optimal RF model performance.

IV. Results and Discussion

Fig.2 shows the BER contour map of the first equalization stage as a function of the equalizer memory length and number of hidden units in the LSTM network for the 125 GHz channel and 300 GHz channel separately. As the network size increases, the equalizer shows improved accuracy in estimating channel impairments, leading to noticeable enhancements in BERs across both channels. However, this enhancement levels off beyond a certain memory length, indicating that the system's nonlinearity is limited within a specific range. Notably,

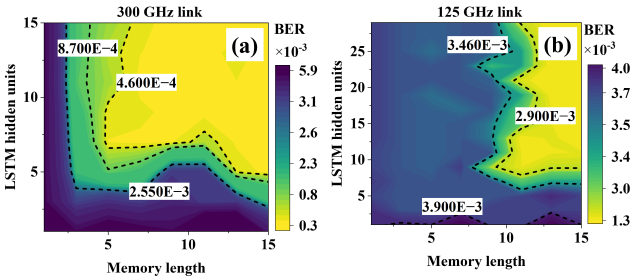

Fig. 2. BER as a function of memory length and number of hidden units for 16 QAM-OFDM signal formats using first equalization stage for (a) 300 GHz channel and (b) 125 GHz channel.

despite employing identical detection schemes, signals, and optical systems, the size of the network and the memory length required to reach saturation level vary between the two channels. Furthermore, the radiated THz power from the PIN-PD at the 125 GHz link is roughly 6 dB higher than that from the UTC-PD at the 300 GHz link, suggesting an expected higher SNR and, therefore, better performance in the 125 GHz link [16]. However, the results do not align with this expectation. This incongruity could be attributed to the lower sensitivity of the FMB detector at 125 GHz. Additionally, unlike the UTC-PD, where only electron carriers contribute to the overall THz photocurrent and, consequently, THz radiation, in the PIN-PD, both hole and electron carriers participate in generating the total THz photocurrent [16]. Nonetheless, due to their higher effective mass, holes are 10 to 20 times slower, which might explain why a larger memory length and network size are required by the 125 GHz link to compensate for the channel distortion. Given the exponential growth in complexity associated with larger networks, the proposed equalizer scheme adopts memory lengths and hidden units of (11,9) and (5,7) for the 125 GHz and 300 GHz links, respectively.

To ensure a comprehensive evaluation, we compared five different frameworks to handle the wave regression task within the first equalization stage. Our candidate frameworks include a two-layer artificial neural network (ANN), a sparse two-layer artificial neural network (S-ANN) with sparsity factors of $\alpha = 0.53$ and $\alpha = 0.48$ for the 125 GHz link and 300 GHz link respectively [17], a conventional third-order Volterra equalizer, and a bidirectional long short-term memory (BiLSTM). It is important to note that all methods underwent optimization using the grid search method, with 25% of the OFDM samples dedicated to training the equalizer. This allocation ensured that

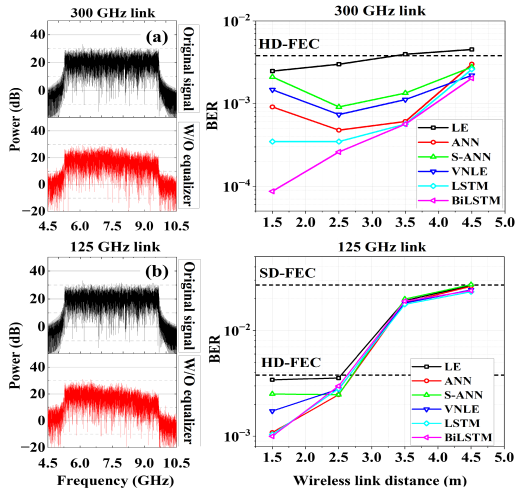

Fig. 3. Frequency spectrum of the OFDM signal before and after passing through the channel, and BER of different frameworks as a function of wireless link distance for (a) 300 GHz channel and (b) 125 GHz channel.

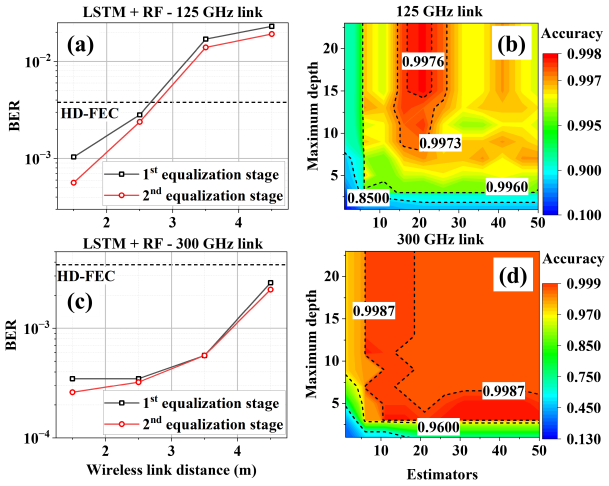

Fig. 4. (a) and (c) BER performance of THz communication system with the first post-equalization block and two-stage NLE for 125 GHz and 300 GHz channels, respectively. (b) and (d) Accuracy of RF classifier as a function of maximum depth and number of estimators for 125 GHz and 300 GHz channels, respectively.

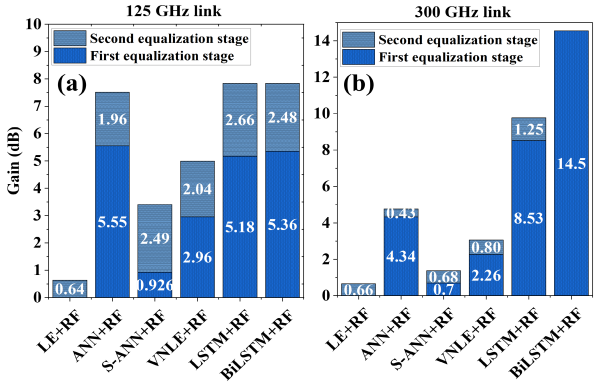

Fig. 5. Gain of the first and second equalization stages separately for different NLE frameworks for (a) 125 GHz channel and (b) 300 GHz channel.

the network captured sufficient channel state information. The optimal number of layers and the number of multiplications, serving as indicators of the framework's complexity, are summarized in Table I.

Fig. 3 presents the performance of different frameworks in terms of BER for various wireless link distances. As shown, BiLSTM provides maximum gain in the 300 GHz link, while in the 125 GHz link, the performance of all ANN, LSTM, and BiLSTM frameworks for 1.5 meters is almost identical. However, with increasing wireless link distance, the performance of all frameworks significantly drops. This could be attributed to free path loss of THz waves and atmospheric attenuation. In general, the effectiveness of a THz wireless link under the LOS scenario heavily relies on its allocated power resources. In shorter link distances, the system's performance is primarily affected by the nonlinearity of the channel. However, as the link distance increases, the signal power decreases quadratically while the noise power remains constant [7]. Eventually, the noise effect on the channel becomes dominant. In this scenario, the system's performance is mainly determined by the power budget rather than systematic nonlinearity. To address this issue, higher optical pump levels can be employed on THz emitters, or THz amplifiers can be utilized.

Despite the initial equalization in the time domain through the first equalization stage, traces of nonlinearity linger in the OFDM signal. In Fig. 3 the spectrum of the transmitted (black) and received (red) 5 Gbaud 16-QAM OFDM signal for both channels can be seen. Without equalization, the received signal experiences significant attenuation at higher frequencies, indicating the presence of frequency-fading effects. This implies that subcarriers with higher frequencies contribute substantially to the overall BER of the system. Fading is more pronounced in the 125 GHz link, accompanied by a lower SNR at longer wireless link distances compared to the 300 GHz link. The first equalization stage compensates for channel effects on the signal by optimizing equalizer hyperparameters to minimize the MSE of the received samples. This means that compensating for faded subcarriers in the first equalization stage is more effective in reducing MSE than compensating for others, resulting in a decreased SNR for other subcarriers.

The limitations of the first equalization scheme in handling this residual nonlinearity prompt the deployment of the second NLE at the sub-carrier level. This secondary NLE discerns nonlinear boundaries between individual QAM symbols and adjusts the standard hard decision thresholds of the 16-QAM demodulator to align with the distribution of received symbols. To determine the optimal number of decision trees in the second post-equalization block and the maximum depth of each individual decision tree, the real and imaginary parts of the received signals are concatenated as two features in the training dataset. A two-dimensional target area is defined for the final decisions. Subsequently, a cross-validation approach, based on the accuracy score, is employed to ascertain the ideal number of decision trees and required depth for classification, as depicted in Fig. 4(b) and (d). The optimal settings for the estimators and the depth of the decision trees are determined to be (20, 20) for the 125 GHz link and (15, 20) for the 300 GHz link. Fig. 4(a) and (c) demonstrates the enhanced performance resulting from the integration of the second post-equalization block for both THz links. The two-stage equalizer effectively improves the communication system's performance by determining optimal decision boundaries.

Fig. 5 compares the gain of the two-stage NLE when utilizing different frameworks under their optimum design.

TABLE I
SUMMARY OF THE COMPLEXITY ATTRIBUTES FOR EACH EQUALIZATION FRAMEWORK

300 GHz							125 GHz						
BiLSTM													
H	L	NM		PT	TT		H	L	NM		PT	TT	
7	5	2595		2.77s	130.08s		7	9	4671		3.1s	137.03s	
LSTM													
H	L	NM		PT	TT		H	L	NM		PT	TT	
7	5	1300		1.31s	114.33s		9	11	4466		1.4s	116.27s	
ANN													
L	N1	N2	N3	NM	PT	TT	L	N1	N2	N3	NM	PT	TT
13	30	30	1	1381	0.5s	120s	15	55	35	1	2876	0.58s	138s
S-ANN													
L	N1	N2	N3	NM	PT	TT	L	N1	N2	N3	NM	PT	TT
13	30	30	1	721	0.4s	108s	15	55	35	1	1339	0.49s	119s
Volterra													
N1	N2	N3	NM				N1	N2	N3	NM			
15	15	15	815				18	18	18	1329			

The gain of the second equalization stage when the first stage is shut down is also provided for reference. As seen from the figure, in both links, BiLSTM+RF offers the best performance. While BiLSTM+RF appears to be the best option in terms of performance, it only tells part of the story. Another important consideration is the complexity of the proposed NLEs. We must balance performance and complexity to achieve high performance while maintaining manageable complexity.

Overall, the total complexity relies on the number of parameters each network must compute, including the number of hidden units and memory length. To directly compare various frameworks, it's essential to compute the computational complexity in terms of the number of real multiplications (NM). For LSTM, this can be calculated as follows [18]:

$$B[H(H+F)+H]L+(H+1)L \tag{4}$$

where $B=4$ for LSTM and 8 for BiLSTM,$F=1$ represents the number of input features, H is the number of hidden units, and L is the memory length of the network. For ANN, we can calculate the number of multiplications as follows:

$$Ln_1+n_1n_2+n_2n_3+n_1+n_2+n_3 \tag{5}$$

where n_1, n_2, and n_3 are the number of hidden units in the corresponding layers.

Table I presents a comparison between the five frameworks in terms of the number of multiplications in both channels, along with their processing time (PT) and training time (TT). All neural network algorithms were implemented using TensorFlow version 2.1.0 and tested on an Nvidia RTX 2060 GPU. Although BiLSTM achieves the best BER performance, its network complexity surpasses all competitors. Conversely, while S-ANN has lower complexity, its performance is inferior. Considering this trade-off between complexity and performance, we opt for a dual-stage NLE with LSTM+RF.

V. CONCLUSION

In this letter, we propose a two-stage nonlinear equalizer scheme employing an LSTM neural network to recognize the pattern of nonlinear behavior in the channel and compensate for it, along with a deep RF network to adjust the decision boundaries of the QAM modulator. This two-stage NLE effectively addresses the linear and nonlinear impairments introduced by the optical and wireless channels on the OFDM signal. Experimental validation on a dual-channel THz-over-fiber system achieves a 20 Gbit/s line rate over a 4.5-meter link at 300 and 125 GHz. The versatility of the proposed method enables its application to various communication systems, effectively compensating for the nonlinear behavior and boosting the performance of the communication channel.

REFERENCES

[1] M. Polese, J. M. Jornet, T. Melodia, and M. Zorzi, "Toward end-to-end, full-stack 6G terahertz networks," *IEEE Commun. Mag.*, vol. 58, no. 11, pp. 48–54, Nov. 2020.

[2] V. Petrov, T. Kurner, and I. Hosako, "IEEE 802.15.3D: First standardization efforts for sub-terahertz band communications toward 6G," *IEEE Commun. Mag.*, vol. 58, no. 11, pp. 28–33, Nov. 2020.

[3] L. Zhang, X. Pang, S. Jia, S. Wang, and X. Yu, "Beyond 100 Gb/s optoelectronic terahertz communications: Key technologies and directions," *IEEE Commun. Mag.*, vol. 58, no. 11, pp. 34–40, Nov. 2020.

[4] C. Wang et al., "Beyond 300-Gbps/λ photonics-aided THz-over-fiber transmission employing MIMO single-carrier frequency-domain equalizer," *Opt. Lett.*, vol. 48, no. 6, pp. 1363–1366, 2023.

[5] A. Morales, G. Nazarikov, S. Rommel, C. Okonkwo, and I. T. Monroy, "Highly tunable heterodyne sub-THz wireless link entirely based on optoelectronics," *IEEE Trans. Terahertz Sci. Technol.*, vol. 11, no. 3, pp. 261–268, May 2021.

[6] H.-H. Lu et al., "Simultaneous transmission of 5G MMW and sub-THz signals through a fiber-FSO-5G NR converged system," *J. Lightw. Technol.*, vol. 40, no. 8, pp. 2348–2356, Apr. 4, 2022.

[7] P. Torkaman et al., "A 5G/Sub-terahertz heterogeneous communication network," *IEEE Access*, vol. 10, pp. 65572–65584, 2022.

[8] M. F. Hermelo, P.-T. B. Shih, M. Steeg, A. Ng'oma, and A. Stöhr, "Spectral efficient 64-QAM-OFDM terahertz communication link," *Opt. Exp.*, vol. 25, no. 16, pp. 19360–19370, Aug. 2017.

[9] K. Li and J. Yu, "Photonics-aided terahertz-wave wireless communication," *J. Lightw. Technol.*, vol. 40, no. 13, pp. 4186–4195, Jul. 9, 2022, doi: 10.1109/JLT.2022.3161878.

[10] M. A. Jarajreh et al., "Artificial neural network nonlinear equalizer for coherent optical OFDM," *IEEE Photon. Technol. Lett.*, vol. 27, no. 4, pp. 387–390, Feb. 4, 2015.

[11] J. Li, Z. Zhang, Y. Wang, B. He, W. Zheng, and M. Li, "Deep learning-assisted OFDM channel estimation and signal detection technology," *IEEE Commun. Lett.*, vol. 27, no. 5, pp. 1347–1351, May 2023.

[12] C. Wang et al., "High-speed terahertz band radio-over-fiber system using hybrid time-frequency domain equalization," *IEEE Photon. Technol. Lett.*, vol. 34, no. 11, pp. 559–562, Jun. 1, 2022, doi: 10.1109/LPT.2022.3171776.

[13] G. S. Yadav, P. Torkaman, X.-W. Miao, K.-M. Feng, and S.-H. Yang, "Performance and complexity analysis using a sparse deep learning method for indoor terahertz transmission," *Opt. Lett.*, vol. 47, no. 17, p. 4431, 2022.

[14] Z. Wang, Z. Xu, J. He, H. Delingette, and J. Fan, "Long short-term memory neural equalizer," *IEEE Trans. Signal Power Integrity*, vol. 2, no. 1, pp. 13–22, Aug. 2023, doi: 10.1109/TSIPI.2023.3242855.

[15] C. Li et al., "Ultra-low complexity random forest for optical fiber communications," *Opt. Exp.*, vol. 31, no. 7, p. 11633, 2023.

[16] S. Nellen et al., "Experimental comparison of UTC- and PIN-photodiodes for continuous-wave terahertz generation," *J. Infr., Millim., Terahertz Waves*, vol. 41, no. 4, pp. 343–354, Apr. 2020.

[17] G. S. Yadav, C.-Y. Chuang, K.-M. Feng, J. Chen, and Y.-K. Chen, "Sparsity learning deep neural network nonlinear equalization method for 112Gbps PAM4 short-reach transmission links," *J. Lightw. Technol.*, vol. 41, no. 8, pp. 2333–2342, Apr. 9, 2023.

[18] S. Deligiannidis, C. Mesaritakis, and A. Bogris, "Performance and complexity analysis of bi-directional recurrent neural network models versus Volterra nonlinear equalizers in digital coherent systems," *J. Lightw. Technol.*, vol. 39, no. 18, pp. 5791–5798, Sep. 4, 2021.